



Hu, X., Wang, H., Faul, C. F. J., Wen, J., Wei, Y., Zhu, M., & Liao, Y. (2020). A crosslinking alkylation strategy to construct nitrogen-enriched tetraphenylmethane-based porous organic polymers as efficient carbon dioxide and iodine adsorbents. *Chemical Engineering Journal*, 382, [122998]. <https://doi.org/10.1016/j.cej.2019.122998>

Peer reviewed version

License (if available):
CC BY-NC-ND

Link to published version (if available):
[10.1016/j.cej.2019.122998](https://doi.org/10.1016/j.cej.2019.122998)

[Link to publication record in Explore Bristol Research](#)
PDF-document

This is the author accepted manuscript (AAM). The final published version (version of record) is available online via Elsevier at <https://www.sciencedirect.com/science/article/pii/S1385894719324088?via%3Dihub>. Please refer to any applicable terms of use of the publisher.

University of Bristol - Explore Bristol Research

General rights

This document is made available in accordance with publisher policies. Please cite only the published version using the reference above. Full terms of use are available: <http://www.bristol.ac.uk/red/research-policy/pure/user-guides/ebr-terms/>

A crosslinking alkylation strategy to construct nitrogen-enriched tetraphenylmethane-based porous organic polymers as efficient carbon dioxide and iodine adsorbents

Xiaowen Hu,¹ Haige Wang,¹ Charl F. J. Faul,² Jin Wen,³ Yen Wei,⁴ Meifang Zhu,¹
Yaozu Liao^{*,1}

¹State Key Laboratory for Modification of Chemical Fibers and Polymer Materials &
College of Materials Science and Engineering, Donghua University, Shanghai
201620, China

²School of Chemistry, University of Bristol, Bristol, England BS8 1TS, UK

³Institute of Organic Chemistry and Biochemistry, Academy of Sciences of the Czech
Republic, Flemingovo nám. 2, 16610 Prague 6, Czech Republic

⁴Department of Chemistry, Tsinghua University, Haidian District, Beijing 100084,
China

Corresponding author. E-mail: yzliao@dhu.edu.cn (Yaozu Liao)

Abstract: Porous organic polymers (POPs) have received great attention worldwide and become attractive for capture and storage of carbon dioxide (CO₂) and radioactive iodine (¹²⁹I or ¹³¹I). Here we present modified tetraphenylmethane (TPM)-based POPs i.e. mPTPMs (synthesized via Buchwald-Hartwig cross-coupling of a tetrakis(4-bromophenyl) methane core and selected aryl diamine linkers, followed by a crosslinking alkylation strategy using diiodomethane as a crosslinker). This new strategy offers mPTPMs with high surface areas up to 640 m²/g and uniform ultramicropore size of 0.6 nm, where porous properties are readily controlled by the substitutions of linkers and the crosslinker. Finally, as-synthesized mPTPMs exhibit

good CO₂ uptake capacities (0.106 g/g at 273 K and 1 bar) and high iodine uptake capacities up to 3.94 g/g within only 2.5 h, representing fast and efficient adsorbents for wider environmental applications.

Keywords: Porous organic polymers, Buchwald-Hartwig cross-coupling, crosslinking alkylation strategy, carbon capture, iodine capture

1. Introduction

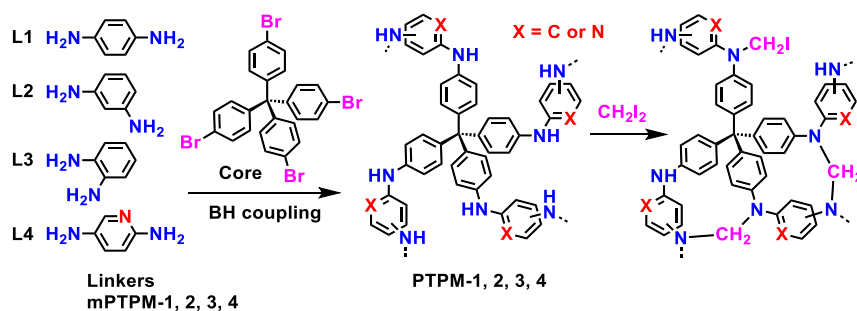
Over the past two decades, the excessive emission of the greenhouse gas carbon dioxide (CO₂) has contributed significantly to global warming and climate change. To stabilize atmospheric CO₂ levels and prevent global warming, many efforts have been devoted to the development of viable CO₂ capture and storage (CCS) technologies.¹ Other routes to avoid CO₂ emission include the development of nuclear technologies for energy generation. These technologies present other challenges in terms of safe storage of nuclear waste, and control of nuclear emissions from these processes. One specific aspect of relevance is the capture of radioactive iodine (I₂), which has also received increasing research interest in the life sciences, marine and atmospheric applications.² Porous organic polymers (POPs), a class of highly crosslinked amorphous polymers with intrinsic nanopores, have recently emerged as a versatile adsorbent platform for the capture and storage of greenhouse CO₂ and radioactive iodine (e.g. ¹²⁹I or ¹³¹I),^{3,4} owing to their facile molecular design, adjustable porosities, tunable surface areas, low skeleton densities, and good physicochemical stabilities.

To achieve both rapid capture and high storage capacity for CO₂ and I₂, a dominant challenge in current POPs research, is the exploration of cost-effective and high surface

area adsorbents bearing high affinities (suitable pore size and functionalities) towards the guest molecules.⁵⁻⁷ Previous studies have shown that alternating the strut lengths, rigidities, and functionalities of the building blocks enable control over the pore size, surface area, and gas uptake of POPs.⁸⁻¹³ For example, tetraphenylmethane (TPM) as an important structural unit has been extensively studied for the construction of a range of POPs because of the default diamondoid framework topology imposed by the tetrahedral monomers.¹⁴⁻²⁰ The unique 3D topology of TPM provides wide openings and interconnected pores to efficiently eliminate “dead space” from the aggregation of polymeric chains.²¹ Versatile TPM-based POPs have been obtained readily through template-free chemical processes by careful selection of building blocks and, commonly, suitable C-C coupling reactions,¹⁴⁻²¹ typically, Sonogashira, Suzuki, and Yamamoto cross-coupling. As expected, many of them exhibit high surface areas and tunable porosities via the careful selection of second building blocks. However, for capture and storage of CO₂ and I₂, these C-C coupling approaches provide mostly materials with limited capacities and selectivities.

In order to improve capacities and selectivities, suitable basic or polar moieties can be deliberately incorporated into the POP backbone. In contrast, the formation of C-N bonds by Buchwald-Hartwig (BH) coupling between amines and aryl halides has become a powerful technique to synthesize POPs.²²⁻²⁵ This useful method provides a simple route to nitrogen-containing polar and redox-active porous materials, showing great potential for the improvement of CO₂ and I₂ capture efficiencies²² as well as electrochemical energy storage.^{24,25} To realize higher surface areas for POPs synthesized via BH coupling, bigger core sizes and longer strut lengths of aryl building blocks are usually required. Under these circumstances, a trade-off between nitrogen

content and surface area is usually found although the nitrogen content of these POPs is still superior to the most of the materials obtained by C-C coupling approaches.



Scheme 1 Modification strategy applied for PTPMs and mPTPMs.

2. Results and discussion

Inspired by these developments, and keen to continue to exploit the BH cross-coupling strategy for POP production, here we extend the nitrogen-containing POP family via the synthesis of novel TPM-based POPs through the BH cross-coupling of the tetrakis(4-bromophenyl)methane (TBPM) core and selected aryl diamine linkers with small size, short strut length, and high nitrogen content (up to 38.5 wt%), i.e., *p*-phenylenediamine (PPDA, **L1**), *m*-phenylenediamine (MPDA, **L2**), *o*-phenylenediamine (OPDA, **L3**), and 2,5-diaminopyridine (DAPD, **L4**, **Scheme 1**). This approach, exploiting careful choice of substitutions and functionalities of the diamine linkers, allow for the formation of 3D amine-linked TPM-based porous organic polymers (PTPMs) i.e. **PTPM-1**, **2**, **3**, and **4**. Post-modification of PTPMs using diiodomethane as a crosslinker, defined here as a “crosslinking alkylation strategy” further leads to the formation of methylene- and iodomethylene-functionalized porous materials, i.e., **mPTPM-1**, **2**, **3** and **4** (**Scheme 1** and **Figure S1**). Although the PTPMs are insoluble in the reaction medium. However, the PTPMs could be readily dispersed in *N,N*-dimethylformamide. The porous structures of PTPMs also allowed the reaction

medium readily to penetrate the polymer networks. Both facts could ensure a successful alkylation. The post-modified mPTPMs show increased surface areas and decreased pore sizes, and maintain high nitrogen content (7-9 wt%) and adjustable electron densities (determined by the density functional theory calculations of their analogues, see details below), finally leading to efficient capture and storage of CO₂ and I₂.

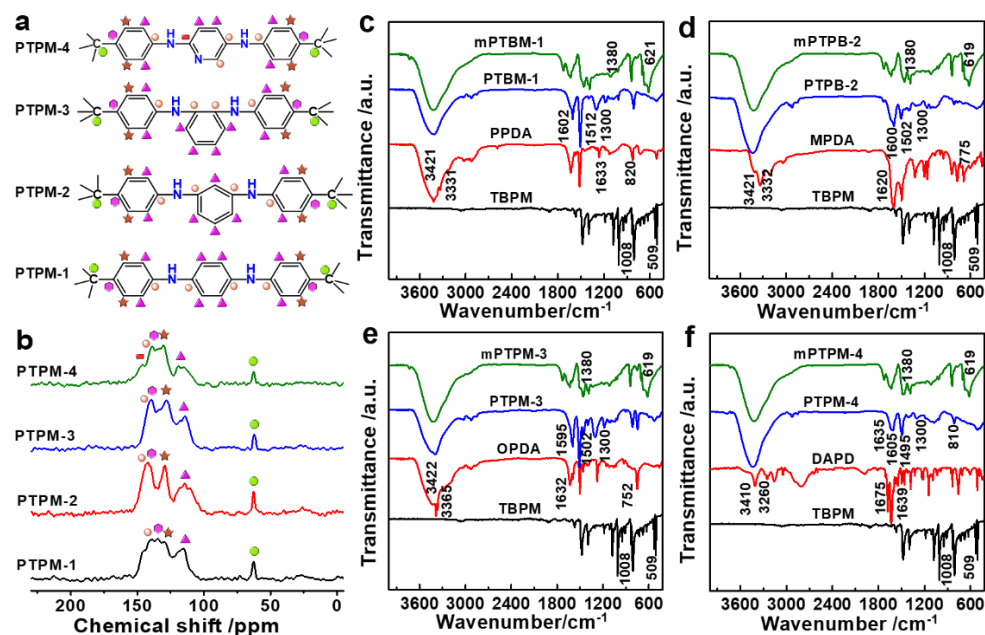


Figure 1 (a) Repeat units, (b) solid-state ¹³C CP/MAS NMR spectra, and (c-f) FT-IR spectra of PTPMs, mPTPMs, and corresponding monomers.

Verification of the structures of PTPMs was achieved by X-ray diffraction (XRD), solid-state ¹³C cross-polarization magic angle spinning nuclear magnetic resonance (CP/MAS NMR), Fourier transform infrared (FT-IR), X-ray photoelectron spectroscopy (XPS), and thermogravimetric analyses. The possible repeat units of PTPMs are presented for the analyses (**Figure 1a**). XRD investigations confirm the amorphous structures of both PTPMs and mPTPMs (**Figure S2**). Solid-state ¹³C CP/MAS NMR spectra of all polymers showed five main resonances at ~63, ~115, ~130, ~136, and ~140 ppm, attributed to the alkyl carbons of TPM group and aryl

carbons in the non-substituted and substituted phenyl groups originating from the starting materials, respectively (**Figure 1b**). An additional resonance at 146 ppm is found for **PTPM-4** and attributed to the pyridine group. The FT-IR spectra indicate that the bands of phenyl C-Br groups of the TBM at 510 and 1010 cm^{-1} (C-Br stretching) and the primary amine group of the linkers at 3421 and 3334 (two sharp bands, $-\text{NH}_2$ stretching) are absent, strongly attenuated or presented as a single broad band in the spectra of the PTPMs (**Figure 1c-f**). The bands of distinct phenyl C-H vibrations with different substitutions (*meta*-, *ortho*-, and *para*-positions) at 752, 775, and 820 cm^{-1} , as well as benzenoid and quinoid bands at 1499 and 1593 cm^{-1} are present in the spectra of the resulting materials. All this information indicates the success of the formation of PTPMs as the structurally indicated in **Scheme 1**. Upon chemically modified using diiodomethane, FT-IR spectra of mPTPMs present a new band at 1380 cm^{-1} ($-\text{CH}_2$ -bending vibration); a band at 1300 cm^{-1} (C-N stretching band) became less intensive, suggesting the successful crosslinking modification. However, all mPTPMs also display a new band at 619 cm^{-1} originating from $-\text{CH}_2\text{I}$, indicating the crosslinking alkylation reaction may not be complete due to the rigidity and steric hindrance of PTPM networks. A full survey XPS spectrum of a typical **mPTPM-3** presents two I3d peaks (**Figure S3**). A high-resolution I3d XPS spectrum shows two single peaks for I3d_{5/2} and I3d_{3/2} at ~620 and 632 eV (**Figure 5c**, see below), respectively, signifying that the iodine is chemically bonded to carbon.²⁶ Moreover, the FT-IR bands near 1500 and 1600 cm^{-1} , characteristic of the stretching vibration of benzenoid and quinoid rings still present in modified polymers i.e. mPTPMs, are slightly shifted. The solid-state ¹³C CP/MAS NMR spectra indicate the alkyl carbons owing to TPM group and methylene group as well as aryl carbons owing to non-substituted and substituted phenyl groups retain in mPTPMs (**Figure S4**). The results suggest the secondary amines were

converted to tertiary amines upon crosslinking, which is in good agreement with previous studies concerning the N-alkylation of polyaniline.²⁷ Upon heating to 800 °C, the PTPMs show good char yields from 68 to 82% owing to their highly crosslinked polymer network structure (**Figure S5**). The mPTPMs are generally much less stable than the parent PTPM materials: they show decreased char yields (60-74%) due to the decomposition of alkylated groups, confirming successful modification. The extents of post-crosslinking were roughly determined by calculating the C/N molar ratios of products on the basis of elemental analyses. The C/N molar ratios for **PTPM-1, 2, 3,** and **4** networks were calculated to be 9.62, 9.62, 9.88, and 7.13; after alkylation, the C/N molar ratios for **mPTPM-1, 2, 3,** and **4** networks were increased to 11.3, 11.57, 12.07, and 8.11, respectively. According to the theoretical C/N molar ratios for **mPTPM-1, 2, 3,** and **4** networks (16.5, 16.5, 16.5, and 10.67), the post-crosslinking extents were therefore calculated to be 68, 70, 73.15, and 76%, respectively. The PTPMs exhibit a nanoparticle morphology, with diameters of 100-150 nm (**Figure S6**). After modifications, the particle sizes decreased to 50-100 nm (**Figure S7**). The diiodomethane could firstly penetrate into the inner of PTPM nanoparticles because of “voids” formed during the polymer growth as confirmed by transmission electron microscope (TEM) observations (**Figure S8**). The methylene as a “crosslinking arm” is bonded to the neighboring amine groups, which led to the observed shrinkage and decrease in particle size (**Figure S9**).

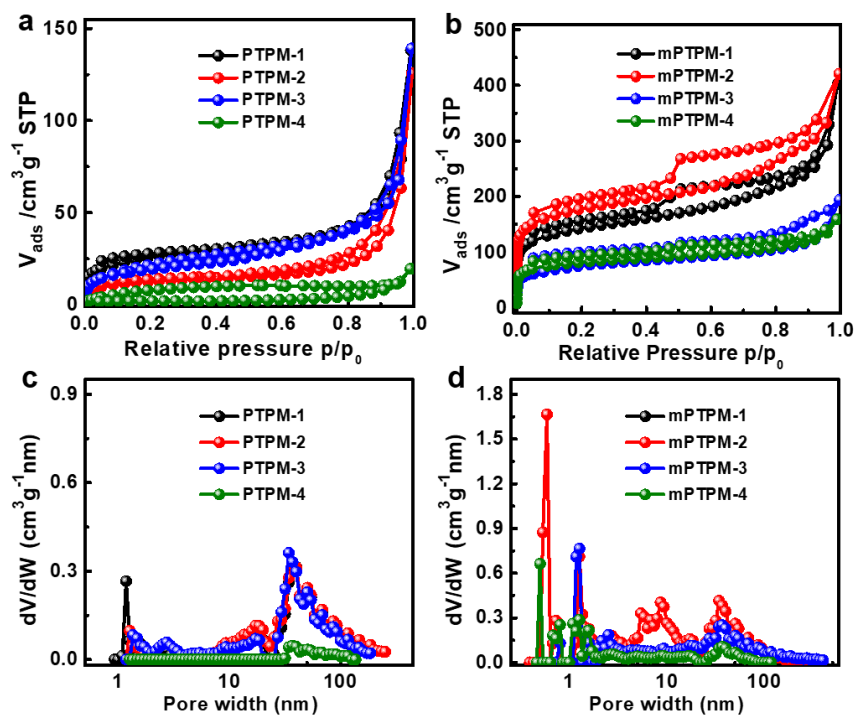


Figure 2 (a,b) N_2 adsorption/desorption isotherms (77 K) and (c,d) DFT pore size distributions of PTPMs and mPTPMs.

According to nitrogen adsorption/desorption isotherm measurements at 77 K, the PTPMs seem not to form a diamondoid cavity because their Brunauer–Emmett–Teller (BET) surface areas ($100 \text{ m}^2/\text{g}$) are much lower than the values obtained on general TPM-based POPs previously reported (**Figure 2a** and **Table 1**).^{14,18} The reason for this observed drop in surface area may be that BH coupling generated amine groups that are not sufficiently rigid to form a diamondoid-like polymer network. However, the amine groups offer suitable affinities towards target gases in this study. They furthermore provide possible sites for modification, therefore offering opportunities for the inclusion of further functionalities and, potentially, higher surface areas. Upon diiodomethane modification, the resulting **mPTPM-1**, **2**, **3**, and **4** show significant increases in BET surface areas of 513, 640, 278, and 293 m^2/g (Langmuir surface areas are 972, 1154, 488, and 495 m^2/g), respectively (**Figure 2b** and **Table 1**). The increased

surface areas are most likely owing to unique “cages” formed via bridging adjacent amine groups, as schematically indicated in **Scheme 1**. The pore size distributions (PSDs) of all the polymer samples were estimated using the quenched solid density function theory (QSDFT) model, confirming the presence of micropores for **PTPM-1**, **2**, and **3** with a pore width of ~1.2 nm, while micropores were not detectable for **PTPM-4** (**Figure 2c** and **Table 1**). Upon the modification, all the mPTPMs present enough micropores to be detected by nitrogen, indicating the increased microporosity. After modification, mPTPMs retain the micropores of ~1.2 nm width, while further micropores with a width of ~0.6 nm have become dominant (**Figure 2d** and **Table 1**). The total pore volumes determined are 0.41, 0.50, 0.21, and 0.20 cm³/g, with micropore volumes of 0.11, 0.15, 0.04, and 0.07 cm³/g for **mPTPM-1**, **2**, **3**, and **4**, respectively, which are both significantly higher than the values obtained from the polymer precursors (see **Table 1**). Beyond that, both PTPMs and mPTPMs present mesopores with a pore width of ~34 nm attributed to the “voids” resulting from nanoparticle aggregation during the polymer growth.¹²

Table 1 Porosities, CO₂ and I₂ uptake properties of PTPMs and mPTPMs.

Sample	S _{BET}	S _{LGM}	^a S _{micro}	^b PV	^c MPV	^d CO ₂	^e I ₂
	(m ² /g)	(m ² /g)	(m ² /g)	(cm ³ /g)	(cm ³ /g)	uptake (g/g)	uptake (g/g)
PTPM-1	94	215	27	0.10	0.01	0.076	1.86
PTPM-2	47	131	17	0.08	0.01	0.06	1.85
PTPM-3	81	222	22	0.09	N/A	0.055	3.22
PTPM-4	37	51	N/A	0.02	N/A	0.037	1.97
mPTPM-1	513	972	265	0.41	0.11	0.085	3.12

mPTPM-2	640	1154	348	0.50	0.15	0.106	3.02
mPTPM-3	278	488	111	0.21	0.04	0.071	3.94
mPTPM-4	293	495	174	0.20	0.07	0.078	2.76

^a t-plot micropore surface area; ^b total pore volume at $p/p_0 = 0.995$; ^c t-plot micropore volume; ^d CO₂ uptake at 273 K and 1 bar; ^e iodine uptake at 358 K for 100 min.

It is widely accepted that the CO₂ uptake capacity at ambient conditions (273-298 K and up to 1 bar) is not only related to the total surface area of the materials but rather on the micropore volume with pore size up to 0.7 nm. The increased surface areas but decreased micropore sizes triggered exploration of their CO₂ capture and storage capabilities using the mPTPMs. The CO₂ adsorption behavior of PTPMs and mPTPMs were measured at 273 and 298 K from lower pressure to 1.0 bar (**Figure 3** and **Table 1**). At 273 K and 1.0 bar, **PTPM-1, 2, 3, and 4** can store 0.076, 0.060, 0.055, and 0.037 g/g of CO₂, respectively. After diiodomethane modifications, **mPTPM-1, 2, 3, and 4** show enhanced CO₂ storage capability, with values of 0.085, 0.106, 0.071, and 0.078 wt%, respectively, under the same conditions. The trends of CO₂ uptake capacities found for PTPMs and mPTPMs are in good agreement with their surface areas. Although the surface areas of mPTPMs are moderate, their CO₂ uptake capacities are still superior to some TPM-based POPs with much higher surface areas (**Table S1**), indicating nitrogen-doped micropores play a curial role in the capture and storage of CO₂.²⁸ Furthermore, to better understand the interaction between CO₂ and the polymer networks, the isosteric heats (Q_{st}) of PTPMs and mPTPMs were calculated based on the Clausius-Clapeyron equation by fitting the CO₂ adsorption isotherms at 273 and 298 K to the virial equation (**Figure 3**).^{11,29} Initial Q_{st} values for CO₂ adsorption are 33.8, 36.8, 32.9, and 35.1 kJ/mol for **PTPM-1, 2, 3, and 4** (**Figure S10**), respectively. After modifications, the Q_{st} values of **mPTPM-1** and **2** decreased (31.7 and 32.9 kJ/mol)

while those of **mPTPM-3** and **4** increased (33.2 and 37.3 kJ/mol, see **Figure S11**). Smaller pore size, larger surface area, and higher basicity of adsorbents have been proven to increase the heat of adsorption.³⁰ The alkylated crosslinking modifications not only decreased the micropore size and increased the surface area but also impaired the basicity of the polymers. The existence of trade-off explains the observed differences in Q_{st} values. Overall, both PTPMs and mPTPMs maintain high Q_{st} values that are superior to most TPM-based POPs previously reported (**Table S1**), indicating that mPTPMs may be exploited as potential adsorbents in CO₂ capture and storage.

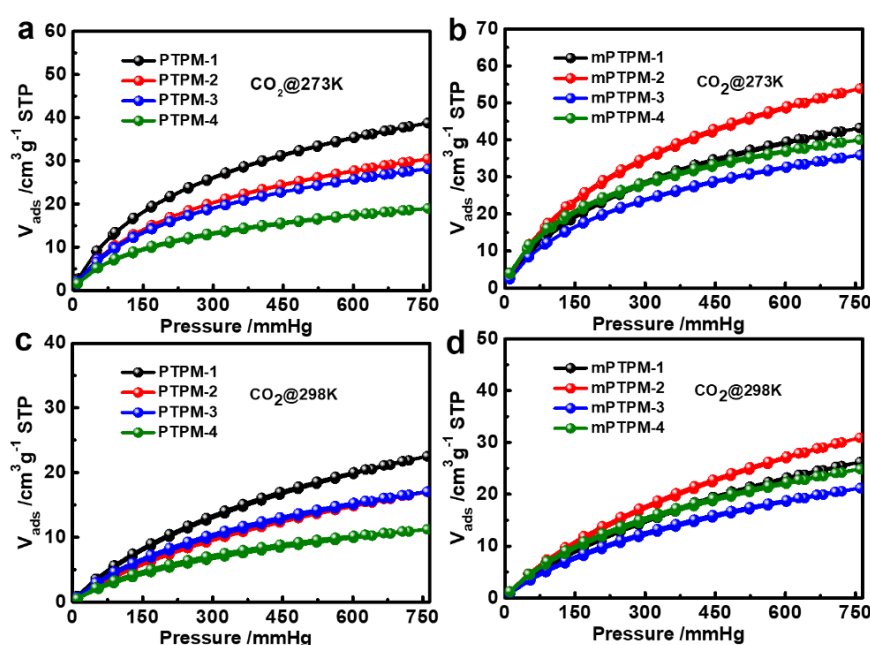


Figure 3 CO₂ adsorption/desorption isotherms of (a,c) PTPMs and (b,d) mPTPMs.

As both PTPM and mPTPM materials exhibited porous characteristics, remarkable stability, and nitrogen-enriched π -conjugated networks, they were used as adsorbents for I₂ uptake. The volatile iodine capture capacities were obtained by gravimetric measurements. These polymer powders were exposed in a closed system filled with excess iodine vapor at 358 K and atmospheric pressure (see the experimental section in Supporting Information for more details). The iodine uptake capacities were recorded

at various time intervals, and the resulting kinetic curves are shown in **Figure 4a,b**. As the exposure continued, the **PTPM-1, 2, and 4** exhibited quick uptake behavior in the initial 30 min and slow uptake within 45-60 min (**Figure 4a**). **PTPM-3** showed an extended initial uptake stage (75 min) and equilibrium uptake stage (75-100 min) (**Figure 4b**). The total uptake capacities at 100 min are 1.86, 1.85, 3.22, and 1.97 g/g for **PTPM-1, 2, 3, and 4**, respectively (**Table 1**).

With the diiodomethane modifications, both initial uptake and equilibrium uptake were extended for the mPTPMs. The total uptake capacities were improved to 3.12, 3.02, 3.94, and 2.76 g/g at 150 min i.e. 2.5 h for **mPTPM-1, 2, 3, and 4**, respectively. Typical examples show that the colors of the polymer samples changed from grey or brown to dark black, supporting their good iodine uptake capacities (**Figure 4c,d**). Different from CO₂ uptake, we found that the iodine uptake capacities of both PTPMs and mPTPMs do not correlate to the surface area or pore volume as determined by gas adsorption/desorption; this behavior is similar to that found for other POPs,^{31,32} metal-organic frameworks (MOFs),³³ and porous carbons.³⁴ The reason for this behavior is that the iodine adsorption in nitrogen-enriched POPs is more akin to chemisorption than the physisorption (found for CO₂ uptake). For chemisorption the functionalities of adsorbents play an even more important role than the surface areas. According to the adsorption kinetic data, the iodine uptake of the polymers fit pseudo-second-order kinetic models well, supporting the assumption of the strong interaction (**Figures S12,13**). The kinetic data show that the rate constant for adsorption in **PTPM-3** is the lowest (**Tables S3,4**), however, the total I₂ uptake is the highest. The adsorption rates are generally determined by the functionalities and interparticle voids of the surface of adsorbents. While the adsorptive uptake capacities are determined by the functionalities, interparticle voids, and surface areas of the bulk of adsorbents. The **PTPM-3** exhibited

the highest electron density (determined by DFT calculations of its analogue, see detailed discussions below) and second highest surface area among the PTPMs, indicating the best accommodative capacities for iodine uptake. This mismatched adsorption behavior might be related to the necessary expansion or swelling of the polymer networks in order to accommodate the iodine molecules.²³ The I₂ uptake capacities of **mPTPM-3** (up to 3.94 g/g within 2.5 h) are superior to most of the reported POPs (**Table S2**), although they are still some little lower than the values found on CaIPOF-1 (4.06 g/g),³⁵ CTF-1@ZnCl₂ (4.31 g/g),³⁶ TatPOP-2 (4.5 g/g),³⁷ and CMP-LS5 (4.1 g/g).³⁸ However, to achieve these values, these adsorbents took significantly longer time (12-30 h), leaving our **mPTPM-3** as a fast and efficient adsorbent for I₂.

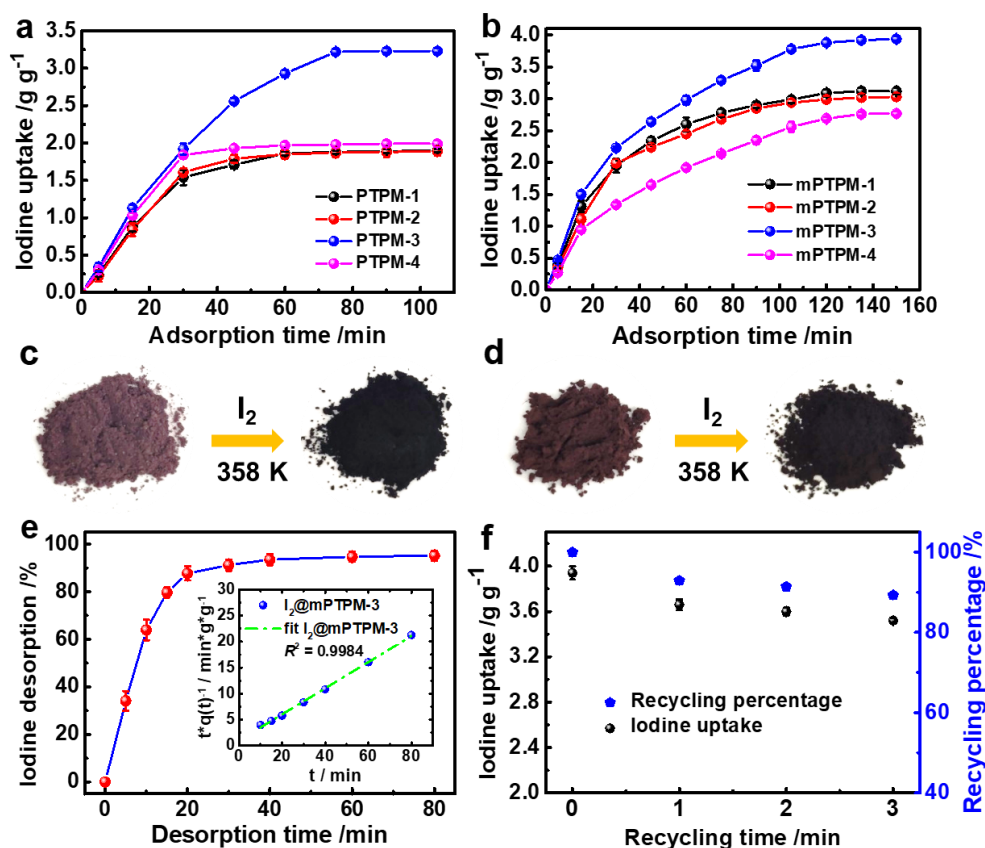


Figure 4 I₂ adsorption curves of (a) PTPMs and (b) mPTPMs; appearance change of (c) PTPM-3 and (d) mPTPM-3 upon iodine adsorption; (e) desorption of I₂ upon heating

I₂@mPTPM-3 at 398 K; inset figure shows kinetic data, pseudo-second-order rate law; and (f) recycling percentage of **mPTPM-3** (recycling parameters: 1.0 bar, 398 K and 60 min).

Previous studies showed that I₂ desorption can be readily induced by heating the I₂-loaded samples at 393-473 K,³⁹⁻⁴¹ providing a facile route to recover the adsorbents. Herein the I₂ desorption and recyclability of the adsorbents were conducted by placing the I₂-loaded samples at 358 K. Taking the **I₂@mPTPM-3** as an example, when heated in air at 398 K and 1.0 bar for 40 min, I₂ desorption efficiency was found to be as high as 93.5% (**Figure 4e**). Interestingly, the thermal desorption also follows pseudo-second-order kinetics (**Figure 4e**, inset). The recovered samples were again used for I₂ adsorption at 358 K and 1 bar to investigate their recyclability (**Figure 4f**). Upon completion of the first cycle, the **mPTPM-3** adsorbent achieved 3.66 g/g uptake capacity, thus retaining ~93% of the initial capacity. After three cycles the **mPTPM-3** adsorbent retains ~90% of the initial capacity with an uptake capacity of 3.53 g/g.

To better understand the interaction between I₂ and the adsorbents, Raman and XPS analyses of **PTPM-3** and **mPTPM-3** upon iodine adsorption were conducted. Before the I₂ adsorption, both **PTPM-3** and **mPTPM-3** display no obvious Raman peaks. After I₂ adsorption, two new Raman bands present a typical “V-shape”, one near 111 cm⁻¹ and one near 166 cm⁻¹ (**Figure 5a,b**).³⁷ Bands in the 110-120 cm⁻¹ range are assigned to the symmetric stretching mode of an I₃⁻ species, while bands near 170 cm⁻¹ are assigned to higher polyiodide anions, i.e. I₅⁻.⁴²

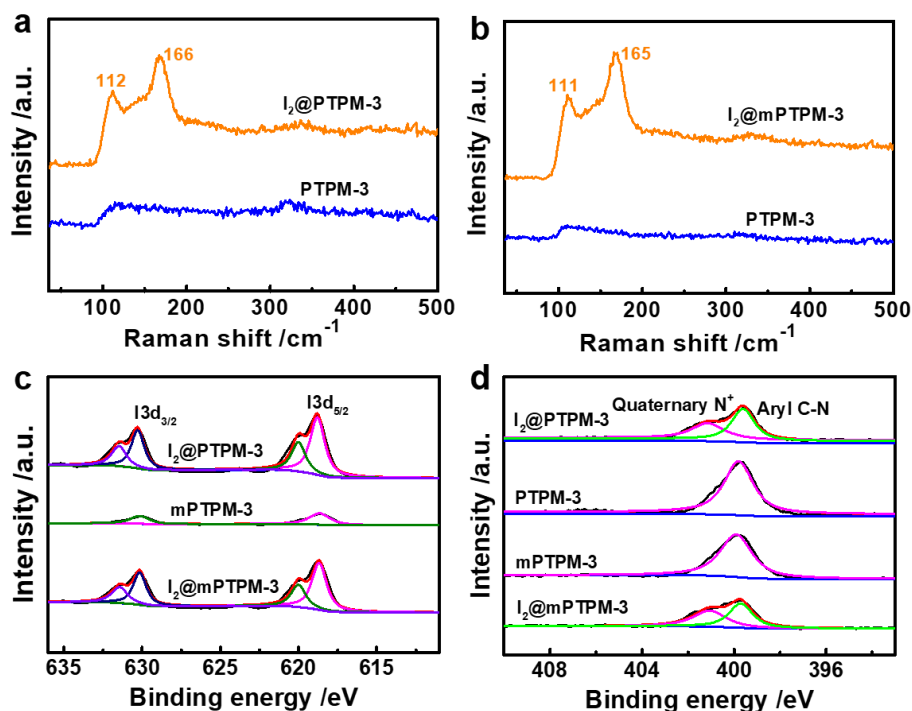


Figure 5 (a,b) Raman, (c) I3d XPS and (d) N1s XPS spectra of **PTPM-3** and **mPTPM-3** upon I₂ adsorption.

The existence of polyiodide anion I₃⁻ and I₅⁻ is further confirmed by X-ray spectral analyses. The I3d XPS spectra of I₂-loaded polymers consisted of two couples of peaks at 632 eV and 620.5 eV for I₅⁻ and 629.8 eV and 618.2 eV for I₃⁻ (**Figure 5c**).⁴³ The **PTPM-3** and **mPTPM-3** exhibit a single N1s XPS peak at 399.8 eV attributed to C-N bond.^{44,45} After adsorption, a new peak at 401.5 eV, originating from a quaternary ammonium cation (N⁺) appears in **I₂@PTPM-3** and **I₂@mPTPM-3** (**Figure 5d**),^{46,47} indicating the presence of a charge transfer (CT) complex between the polymer networks and polyiodide anions. As the tertiary amine has a higher affinity to form CT complexes with I₂ (compared with the secondary amine), it provides an explanation for the much improved I₂ uptake capacities found upon the alkylation modifications. It can therefore be concluded that the I₂ is chemically attached to the polymeric adsorbents

(see the adsorptive model in **Figure S14**), with such chemisorptive processes in accordance with the pseudo-second-order adsorption kinetics described above.

As chemical interactions play a leading role in the iodine adsorption, obtaining insight into the electron densities of the nitrogen atoms of polymers can help to understand the mechanism of how choice of building blocks and alkylation influence iodine uptake capacities and adsorption. For this purpose, eight molecular models as analogs of the **PTPMs** and **mPTPMs** were used to predict the electron densities of the nitrogen atoms on the basis of DFT calculations (**Figure 6**, **Figure S15**, and **Table S5**). Clearly, the *ortho*-substitution and alkylation enhanced the electron densities on the nitrogen atoms, leading to the enhanced I₂ uptake. The electron densities of nitrogen atoms are evaluated by the projections of its two-dimensional maps onto their long axes, noted as *y* axes in **Figure 6a,c**. The electron densities of nitrogen atoms were found to be approximately 20 and 23 $e^- \text{Å}^{-1}$ in the models for **PTPM-3** and **mPTPM-3**, respectively, which agrees well with their highest iodine uptake capacities. We can therefore conclude that these findings provide useful guidance for future rational design of polymeric adsorbents for iodine capture.

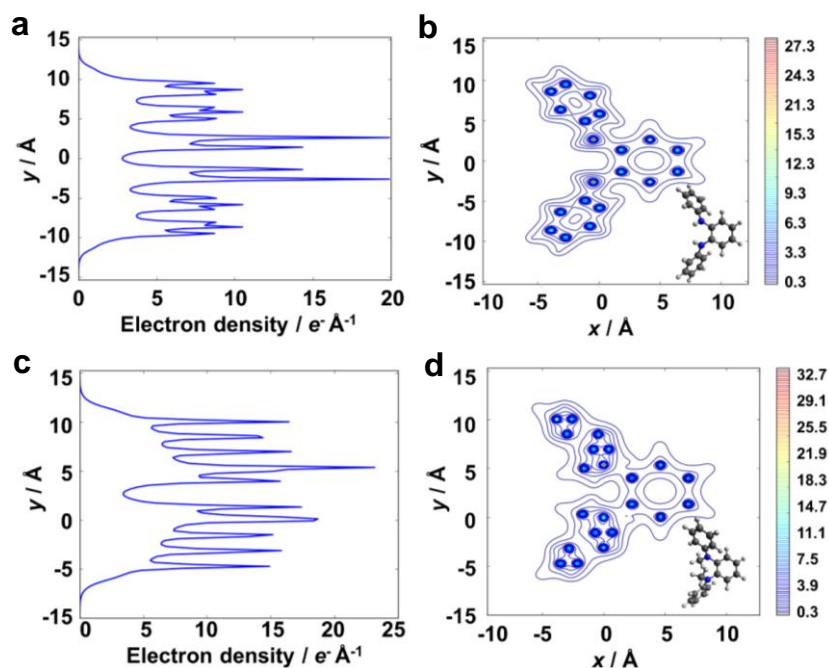


Figure 6 Electron density profiles for analogs of (a,b) **PTPM-3**, and (c,d) **mPTPM-3** in DFT calculations. Chemical structures are shown in the insets of (b) and (d).

3. Conclusions

A series of nitrogen-rich porous organic polymers (POPs) were successfully synthesized through the Buchwald-Hartwig cross-coupling of a tetrakis(4-bromophenyl)methane core and selected aryl diamine linkers. Post-synthetic modification using diiodomethane as a crosslinker was further explored to form methylene- and iodomethylene-functionalized porous materials. The mPTPMs constructed from the crosslinking alkylation strategy showed increased specific surface areas (640 m²/g) and decreased pore sizes (0.6 nm), and maintained high nitrogen contents (~9 wt%), finally leading to improved CO₂ (0.106 g/g) and iodine uptake capacities (3.94 g/g). Kinetic studies indicated the CO₂ and I₂ uptakes follow physically and chemically adsorptive mechanisms, respectively. Upon crosslinking modifications, the increased surface and decreased micropore size correspond to the improved CO₂ uptake capacities, whilst the alkylation, as well as the ortho-substitution of the building

blocks, play a more critical role to enhance iodine uptake capacities. Furthermore, porous adsorbents presented here could be recovered with minimal (only 10%) loss of iodine uptake capacity. Our results demonstrate that optimization of starting building blocks, cross-coupling methods, and post-synthetic modifications offer promising adsorbents for capture and sequestration of greenhouse and harmful gases to address global environmental challenges.

Acknowledgments

We acknowledge the financial support from the Fundamental Research Funds for the Central Universities (2232019A3-01), the National Natural Science Foundation of China (51873036 and 51673039), the Shanghai Natural Science Foundation (19ZR1470900), the Shanghai Shuguang Program (19SG28), and the International Joint Laboratory for Advanced fiber and Low-Dimension Materials (18520750400).

References

1. Scott, V.; Gilfillan, S.; Markusson, N.; Chalmers, H.; Haszeldine, R. S. Last Chance for Carbon Capture and Storage. *Nat. Clim. Change*. **2013**, *3*, 105-111.
2. Huve, J.; Ryzhikov, A.; Nouali, H.; Lalia, V.; Augé, G.; Daou, T. J. Porous Sorbents for the Capture of Radioactive Iodine Compounds: A Review. *RSC Adv*. **2018**, *8*, 29248-29273.
3. Chaoui, N.; Trunk, M.; Dawson, R.; Schmidt, J.; Thomas, A. Trends and Challenges for Microporous Polymers. *Chem. Soc. Rev*. **2017**, *46*, 3302-3321.
4. Zou, L.; Sun, Y.; Che, S.; Yang, X.; Wang, X.; Bosch, M.; Perry, Z. Porous Organic Polymers for Post-Combustion Carbon Capture. *Adv. Mater*. **2017**, *29*, 1700229.
5. Wang, W.; Zhou, M.; Yuan, D. Carbon Dioxide Capture in Amorphous Porous Organic Polymers. *J. Mater. Chem. A* **2017**, *5*, 1334-1347.

-
6. Tan, L.; Tan, B. Hypercrosslinked Porous Polymer Materials: Design, Synthesis, and Applications. *Chem. Soc. Rev.* **2017**, *46*, 3322-3356.
 7. Sun, Q.; Aguila, B.; Ma, S. Opportunities of Porous Organic Polymers for Radionuclide Sequestration. *Trends Chem.* **2019**, *1*, 292-303.
 8. Alsbaiee, A.; Smith, B. J.; Xiao, L.; Ling, Y.; Helbling, D. E.; Dichtel, W. R. Rapid Removal of Organic Micropollutants from Water by a Porous β -Cyclodextrin Polymer. *Nature* **2016**, *529*, 190-194.
 9. Bildirir, H.; Gregoriou, V. G.; Avgeropoulos, A.; Scherf, U.; Chochos, C. L. Porous Organic Polymers as Emerging New Materials for Organic Photovoltaic Applications: Current Status and Future Challenges. *Mater. Horiz.* **2017**, *4*, 546-556.
 10. Zhu, J.; Yang, C.; Lu, C.; Zhang, F.; Yuan, Z.; Zhuang, X. Two-Dimensional Porous Polymers: From Sandwich-like Structure to Layered Skeleton. *Acc. Chem. Res.* **2018**, *51*, 3191-3202.
 11. Liao, Y.; Cheng, Z.; Zuo, W.; Thomas, A.; Faul, C. F. Nitrogen-Rich Conjugated Microporous Polymers: Facile Synthesis, Efficient Gas Storage, and Heterogeneous Catalysis. *ACS Appl. Mater. Interfaces* **2017**, *9*, 38390-38400.
 12. Liao, Y.; Weber, J.; Faul, C. F. Fluorescent Microporous Polyimides Based on Perylene and Triazine for Highly CO₂-Selective Carbon Materials. *Macromolecules* **2015**, *48*, 2064-2073.
 13. Li, H.; Li, J.; Thomas, A.; Liao, Y. Ultra-High Surface Area Nitrogen-Doped Carbon Aerogels Derived From a Schiff-Base Porous Organic Polymer Aerogel for CO₂ Storage and Supercapacitors. *Adv. Funct. Mater.* **2019**, 1904785.
 14. Yuan, Y.; Zhu, G. Porous Aromatic Frameworks as a Platform for Multifunctional Applications. *ACS Cent. Sci.* **2019**, *5*, 409-418.

-
15. Lu, W.; Yuan, D.; Zhao, D.; Schilling, C. I.; Plietzsch, O.; Muller, T.; Li, Z. Porous Polymer Networks: Synthesis, Porosity, and Applications in Gas Storage/Separation. *Chem. Mater.* **2010**, *22*, 5964-5972.
16. Ren, H.; Ben, T.; Wang, E.; Jing, X.; Xue, M.; Liu, B.; Zhu, G. Targeted Synthesis of a 3D Porous Aromatic Framework for Selective Sorption of Benzene. *Chem. Commun.* **2010**, *46*, 291-293.
17. Thiel, K.; Zehbe, R.; Roeser, J.; Strauch, P.; Enthaler, S.; Thomas, A. A Polymer Analogous Reaction for the Formation of Imidazolium and NHC Based Porous Polymer Networks. *Polym. Chem.* **2013**, *4*, 1848-1856.
18. Ben, T.; Ren, H.; Ma, S.; Cao, D.; Lan, J.; Jing, X.; Qiu, S. Targeted Synthesis of a Porous Aromatic Framework with High Stability and Exceptionally High Surface Area. *Angew. Chem. Int. Ed.* **2009**, *48*, 9457-9460.
19. Uptmoor, A. C.; Geyer, F. L.; Rominger, F.; Freudenberg, J.; Bunz, U. H. Tetrahedral Tetrakis(p-ethynylphenyl) Group IV Compounds in Microporous Polymers: Effect of Tetrel on Porosity. *ChemPlusChem* **2018**, *83*, 448-454.
20. Li, L.; Ren, H.; Yuan, Y.; Yu, G.; Zhu, G. Construction and Adsorption Properties of Porous Aromatic Frameworks via AlCl₃-Triggered Coupling Polymerization. *J. Mater. Chem. A* **2014**, *2*, 11091-11098.
21. Yuan, D.; Lu, W.; Zhao, D.; Zhou, H. C. Highly Stable Porous Polymer Networks with Exceptionally High Gas-Uptake Capacities. *Adv. Mater.* **2011**, *23*, 3723-3725.
22. Liao, Y.; Weber, J.; Faul, C. F. Conjugated Microporous Polytriphenylamine Networks. *Chem. Commun.* **2014**, *50*, 8002-8005.
23. Liao, Y.; Weber, J.; Mills, B. M.; Ren, Z.; Faul, C. F. Highly Efficient and Reversible Iodine Capture in Hexaphenylbenzene-Based Conjugated Microporous Polymers. *Macromolecules* **2016**, *49*, 6322-6333.

-
24. Liao, Y.; Wang, H.; Zhu, M.; Thomas, A. Efficient Supercapacitor Energy Storage Using Conjugated Microporous Polymer Networks Synthesized from Buchwald-Hartwig Coupling. *Adv. Mater.* **2018**, *30*, 1705710.
25. Bandyopadhyay, S.; Singh, C.; Jash, P.; Hussain, M. W.; Paul, A.; Patra, A. Redox-Active, Pyrene-Based Pristine Porous Organic Polymers for Efficient Energy Storage with Exceptional Cyclic Stability. *Chem. Commun.* **2018**, *54*, 6796-6799.
26. Cheng, F.; Wu, X. J.; Hu, Z.; Lu, X.; Ding, Z.; Shao, Y.; Loh, K. P. Two-Dimensional Tessellation by Molecular Tiles Constructed from Halogen-Halogen and Halogen-Metal Networks. *Nat. Commun.* **2018**, *9*, 4871.
27. Zheng, W. Y.; Levon, K.; Laakso, J.; Oesterholm, J. E. Characterization and Solid-State Properties of Processable N-alkylated Polyanilines in the Neutral State. *Macromolecules* **1994**, *27*, 7754-7768.
28. Yuan, K. Y.; Liu, C. D.; Liu, C.; Zhang, S. H.; Yu, G. P.; Yang, L.; Yang, F. H.; Jian, X. G. Construction of Triphenylamine Functional Phthalazinone-Based Covalent Triazine Frameworks for Effective CO₂ Capture. *Polymer* **2018**, *151*, 65-74.
29. Sevilla, M.; Fuertes, A. B. Sustainable Porous Carbons with a Superior Performance for CO₂ Capture. *Energy Environ. Sci.* **2011**, *4*, 1765-1771.
30. Liao, Y.; Cheng, Z.; Truck, M.; Thomas, A. Targeted Control Over the Porosities and Functionalities of Conjugated Microporous Polycarbazole Networks for CO₂-Selective Capture and H₂ Storage. *Polym. Chem.* **2017**, *8*, 7240-7247.
31. Weber, J.; Antonietti, M.; Thomas, A. Microporous Networks of High-Performance Polymers: Elastic Deformations and Gas Sorption Properties. *Macromolecules* **2008**, *41*, 2880-2885.
32. Schmidt, J.; Weber, J.; Epping, J. D.; Antonietti, M.; Thomas, A. Microporous Conjugated Poly(thienylene arylene) Networks. *Adv. Mater.* **2009**, *21*, 702-705.

-
33. Falaise, C.; Volkringer, C.; Facqueur, J.; Bousquet, T.; Gasnot, L.; Loiseau, T. Capture of Iodine in Highly Stable Metal-Organic Frameworks: A Systematic Study. *Chem. Commun.* **2013**, *49*, 10320-10322.
34. Subrahmanyam, K. S.; Sarma, D.; Malliakas, C. D.; Polychronopoulou, K.; Riley, B. J.; Pierce, D. A.; Chun, J.; Kanatzidis, M. G. Chalcogenide Aerogels as Sorbents for Radioactive Iodine. *Chem. Mater.* **2015**, *27*, 2619-2626.
35. Su, K.; Wang, W.; Li, B.; Yuan, D. Azo-Bridged Calix[4]resorcinarene-Based Porous Organic Frameworks with Highly Efficient Enrichment of Volatile Iodine. *ACS Sustainable Chem. Eng.* **2018**, *6*, 17402-17409.
36. He, X.; Zhang, S. Y.; Tang, X.; Xiong, S.; Ai, C.; Chen, D.; Yu, G. Exploration of 1D Channels in Stable and High-Surface-Area Covalent Triazine Polymers for Effective Iodine Removal. *Chem. Eng. J.* **2019**, *371*, 314-318.
37. Xiong, S. H.; Tao, J.; Wang, Y. Y.; Tang, J. T.; Liu, C.; Liu, Q. Q.; Wang, Y.; Yu, G. P.; Pan, C. Y. Uniform Poly(phosphazene-triazine) Porous Microspheres for Highly Efficient Iodine Removal. *Chem. Commun.* **2018**, *54*, 8450-8453.
38. Wang, S.; Liu, Y.; Ye, Y.; Meng, X.; Du, J.; Song, X.; Liang, Z. Ultrahigh Volatile Iodine Capture by Conjugated Microporous Polymer Based on N, N, N', N'-tetraphenyl-1, 4-phenylenediamine. *Polym. Chem.* **2019**, *10*, 2608-2615.
39. Geng, T.; Ye, S.; Zhu, Z.; Zhang, W. Triazine-Based Conjugated Microporous Polymers with N,N,N',N'-Tetraphenyl-1,4-Phenylenediamine, 1,3,5-Tris(diphenylamino)benzene and 1,3,5-Tris[(3-Methylphenyl)-Phenylamino] benzene as the Core for High Iodine Capture and Fluorescence Sensing of o-Nitrophenol. *J. Mater. Chem. A* **2018**, *6*, 2808-2816.
40. Janeta, M.; Bury, W.; Szafert, S. Porous Silsesquioxane-Imine Frameworks as Highly Efficient Adsorbents for Cooperative Iodine Capture. *ACS Appl. Mater.*

Interfaces **2018**, *10*, 19964-19973.

41. Li, B.; Wang, B.; Huang, X.; Dai, L.; Cui, L.; Li, J.; Li, C. Terphen[n]arenes and Quaterphen[n]arenes (n=3-6): One-Pot Synthesis, Self-Assembly into Supramolecular Gels, and Iodine Capture. *Angew. Chem. Int. Ed.* **2019**, *58*, 3885-3889.
42. Zur Loye, H. C.; Heyen, B. J.; Marcy, H. O.; DeGroot, D. C.; Kannewurf, C. R.; Shriver, D. F. Dielectric Response and Conductivity of Poly(propylene oxide) Sodium Polyiodide Complexes. Discussion of Charge Transport by An Ion Relay Mechanism. *Chem. Mater.* **1990**, *2*, 603-609.
43. Zhu, Y.; Ji, Y. J.; Wang, D. G.; Zhang, Y.; Tang, H.; Jia, X. R.; Kuang, G. C. BODIPY-Based Conjugated Porous Polymers for Highly Efficient Volatile Iodine Capture. *J. Mater. Chem. A* **2017**, *5*, 6622-6629.
44. Ma, L.; Zhuang, H. L.; Wei, S.; Hendrickson, K. E.; Kim, M. S.; Cohn, G.; Archer, L. A. Enhanced Li-S Batteries Using Amine-Functionalized Carbon Nanotubes in the Cathode. *ACS Nano* **2016**, *10*, 1050-1059.
45. Li, X. C.; Zhang, Y.; Wang, C. Y.; Wan, Y.; Lai, W. Y.; Pang, H.; Huang, W. Redox-Active Triazatruxene-Based Conjugated Microporous Polymers for High-Performance Supercapacitors. *Chem. Sci.* **2017**, *8*, 2959-2965.
46. Sun, Y.; Chen, C.; Xu, H.; Lei, K.; Xu, G.; Zhao, L.; Lang, M. Surface Modification of Silicon Wafer by Grafting Zwitterionic Polymers to Improve Its Antifouling Property. *Appl. Surf. Sci.* **2017**, *419*, 642-649.
47. Li, S. W.; Yang, Z.; Gao, R. M.; Zhang, G.; Zhao, J. S. Direct Synthesis of Mesoporous SRL-POM@MOF-199@MCM-41 and Its Highly Catalytic Performance for the Oxidesulfurization of DBT. *Appl. Catal., B: Environ.* **2018**, *221*, 574-583.

Table of contents entry

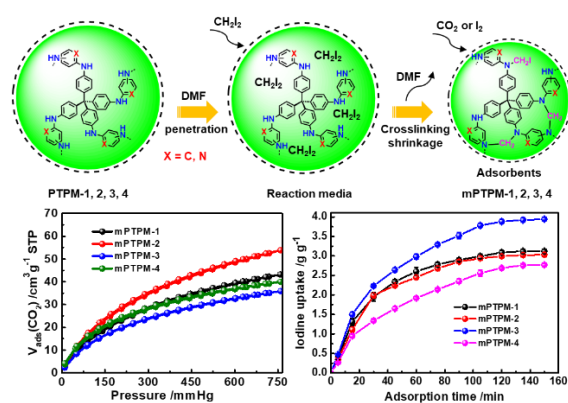
The construction of nitrogen-enriched porous organic polymers by a novel crosslinking alkylation strategy enables efficient capture and storage of greenhouse carbon dioxide and radioactive iodine to address global environmental challenges.

Keywords: Porous organic polymers, Buchwald-Hartwig cross-coupling, crosslinking alkylation strategy, carbon capture, iodine capture

Authors: Xiaowen Hu, Haige Wang, Charl F. J. Faul, Jin Wen, Yen Wei, Meifang Zhu, Yaozu Liao

Title: A crosslinking alkylation strategy to construct nitrogen-enriched tetraphenylmethane-based porous organic polymers as efficient carbon dioxide and iodine adsorbents

ToC figure:



A crosslinking alkylation strategy to construct nitrogen-enriched tetraphenylmethane-based porous organic polymers as efficient carbon dioxide and iodine adsorbents

Xiaowen Hu,¹ Haige Wang,¹ Charl F. J. Faul,² Jin Wen,³ Yen Wei,⁴ Meifang Zhu,¹
Yaozu Liao^{*,1}

¹State Key Laboratory for Modification of Chemical Fibers and Polymer Materials &
College of Materials Science and Engineering, Donghua University, Shanghai
201620, China

²School of Chemistry, University of Bristol, Bristol, England BS8 1TS, UK

³Institute of Organic Chemistry and Biochemistry, Academy of Sciences of the Czech
Republic, Flemingovo nám. 2, 16610 Prague 6, Czech Republic

⁴Department of Chemistry, Tsinghua University, Haidian District, Beijing 100084,
China

Corresponding author. E-mail: yzliao@dhu.edu.cn (Yaozu Liao)

Table of Content

S1. Experimental Section

S1.1. Materials

S1.2. Synthesis of amine-linked porous organic polymers

S1.3. Chemical modification of amine-linked porous organic polymers

S2. Characterization and Measurements

S2.1. Structure and morphology characterization

S2.2. N₂ and CO₂ adsorption/desorption measurements

S2.3. Iodine adsorption/desorption measurements

S2.4. Density functional theory (DFT) calculations

S3. Supplementary Figures and Tables

S4. Supplementary References

1. Experimental Section

1.1. Materials

Tetrakis(4-bromophenyl)methane (TBM, >97%), *p*-phenylenediamine (PPDA, >98%), *m*-phenylenediamine (MPDA, >98%), *o*-phenylenediamine (OPDA, >98%), 2,5-diaminopyridine (DAPD, >98%), bis(dibenzylideneacetone)palladium(0) (Pd(dba)₂, 18-24% Pd), 2-dicyclohexylphosphino-2',4',6'-triisopropylbiphenyl (XPhos, >98%), sodium *tert*-butoxide (NaOtBu, >98%), iodine solids (≥99.8%), and all the solvents with A.R and C.R. grades were purchased from Tokyo Chemical Industry Ltd., Shanghai.

1.2. Synthesis of amine-linked porous organic polymers

The amine-linked porous organic polymers were synthesized via a Buchwald-Hartwig coupling reaction. Typically, a Schlenk tube was charged with TBM (1 mmol, 1 equiv.), diamine (2 mmol, 2 equiv., *p*-phenylenediamine **L1**, *m*-phenylenediamine **L2**, *o*-phenylenediamine **L3**, or 2,5-diaminopyridine **L4**), Pd(dba)₂ (46 mg, 0.08 mmol, 8 mol%), XPhos (57.2 mg, 0.125 mmol, 12 mol%), and NaOtBu (480.5 mg, 5 mmol, 5 equiv.) and placed under a nitrogen atmosphere. Anhydrous toluene (150 mL) was

added and the reaction mixture was heated under stirring to 110 °C. After 24 h, the reaction was cooled to room temperature and products separated by centrifugation. The remaining solids were washed by chloroform, hot deionized water (65 °C) and methanol (3 × 200 mL), and then dried 72 h in a vacuum oven to yield the corresponding **PTPM-1, 2, 3, and 4** networks as dark-brown, brownish green, gray, and brown powders with yields of 86.9, 67.3, 77.3, and 73.5%, respectively. *Anal. Found* for **PTPM-1**: C, 80.8; N, 9.8; H, 5.7; *Anal. Found* for **PTPM-2**: C, 78.3; N, 9.5; H, 5.4; *Anal. Found* for **PTPM-3**: C, 77.9; N, 9.2; H, 5.6; *Anal. Found* for **PTPM-4**: C, 74.6; N, 12.2; H, 5.0. The C/N molar ratios for **PTPM-1, 2, 3, and 4** networks were calculated to be 9.62, 9.62, 9.88, and 7.13, respectively.

1.3. Chemical modification of amine-linked porous organic polymers

A crosslinking alkylation strategy was applied to modify the amine-linked porous organic polymers using diiodomethane as the linker. Typically, **PTPM-1, 2, 3, or 4** (110 mg) and potassium carbonate (691 mg, 5 mmol) were thoroughly mixed and ground for 10 min. The powder mixture and *N,N*-dimethylformamide (50 mL) was placed in a three-necked flask and then vigorously shaken for 60 min. Finally, diiodomethane (643 mg, 2.4 mmol) was added under a nitrogen atmosphere and the reaction mixture was heated under stirring to 152 °C. After 24 h, the reaction was cooled to room temperature and products separated by centrifugation. The remaining solids were washed by *N,N*-dimethylformamide, hot deionized water (65 °C) and methanol (3 × 200 mL), and then dried 72 h in a vacuum oven to yield the corresponding **mPTPB-1, 2, 3, and 4** networks as reddish brown, brown, dark brown, and orange powders with yields of 61.5, 42.3, 56.4, and 50.6%, respectively. *Anal. Found* for **mPTPM-1**: C, 73.7; N, 7.6; H, 4.5; *Anal. Found* for **mPTPM-2**: C, 74.4; N, 7.5; H, 4.6; *Anal. Found* for **mPTPM-3**: C, 74.5; N, 7.2; H, 4.7; *Anal. Found* for **mPTPM-4**: C, 72.6; N, 9.3; H,

4.7. The C/N molar ratios for **mPTPM-1, 2, 3,** and **4** networks were calculated to be 11.3, 11.57, 12.07, and 9.11, respectively.

2. Characterization and Measurements

2.1. Structure and morphology characterization

Fourier transform infrared (FT-IR) spectra were taken on a Nicolet 670 spectrometer. Solid-state ^{13}C cross-polarization magic angle spinning nuclear magnetic resonance (CP/MAS NMR) spectra were taken on an AVANCE400 spectrometer. X-ray photoelectron spectra (XPS) were obtained on a PHI5000 1 Versa probe-II multifunctional 2 scanning and imaging photoelectron spectrometer equipped with an Al $K\alpha$ X-ray source. Powder X-ray diffraction (XRD) patterns were obtained on a Bruker D8 Advance diffractometer using Cu $K\alpha$ radiation ($2\theta = 5-90^\circ$). Laser Raman spectra were characterized by an inVia Reflex spectrometer (532 nm, 0.05%, 1 s). Thermal gravimetric analysis (TGA) was carried out on a TGA Q500 apparatus under a nitrogen atmosphere in a temperature range 30-900 °C (heating rate 10 °C/min). Scanning electron microscope (SEM) images were obtained on a HITACHI S-4800 and transmission electron microscope (TEM) images were obtained on a JEM-2100 TEM microscope.

2.2. N_2 and CO_2 adsorption/desorption measurements

N_2 adsorption/desorption measurements at 77 K were performed after degassing the samples under a high vacuum at 343 K for at least 20 hours using a Micro VacPrep061 machine. CO_2 adsorption/desorption isotherms at 273 and 298 K were conducted on a Micro ASAP2046 machine after prior degassing under high vacuum at 343 K. The specific surface areas were calculated by applying the Brunauer-Emmett-Teller (BET)

model to adsorption or desorption branches of the isotherms (N₂ at 77 K) using the Micro for ASAP2460 software package. The non-local density functional theory (NLDFT) model was used to calculate the pore size distribution. The heat of CO₂-adsorption was calculated via the Clausius–Clapeyron method on the basis of the CO₂ adsorption/desorption isotherms obtained at 273 and 298 K.

2.3. Iodine adsorption/desorption measurements

Iodine (I₂) uptake experiments were performed based on gravimetric measurements; the procedure was conducted as follows. 10 mg of PTPM or mPTPM powder charged in an open thermoresistant plastic pan (1 mL) and 1 g of I₂ solids were placed in a sealed glass vial (20 mL) and heated at 358 K and 1.0 bar to generate I₂ vapor. After adsorption for a while (0-105 min), I₂-loaded polymer powder was cooled down to room temperature and weighted. The I₂ uptake capacities for PTPMs or mPTPMs were calculated by weight gains: $c_u = (m_2 - m_1) / m_1 \times 100$ wt%, where c_u is the I₂ uptake capacity, m_1 and m_2 are the mass weight of adsorbents before and after adsorption. I₂ release and adsorbent recycles were conducted as follows: typically, 10 mg of I₂-equilibrium **mPTPM-3** (c_u : 394 wt%) powder containing 7.98 mg iodine charged in an open thermoresistant plastic pan (1 mL) was placed in an open glass vial (20 mL) and heated at 398 K and 1.0 bar in an oil bath for 80 min. The I₂ release efficiency was calculated by weight gains: $e_r = (10 - m_t) / 7.98 \times 100$ wt%, where e_r is the I₂ release efficiency, m_t is the mass weight of **mPTPM-3** after heating. Recycling percentage (r_p) of the adsorbents was determined as follows: 30 mg of I₂-equilibrium **mPTPM-3** (c_u : 394 wt%, 3.94 g g⁻¹) powder charged in an open thermoresistant plastic pan (1 mL) was placed in an open glass vial (20 mL) and heated at 398 K and 1.0 bar for 80 min in an oil bath. The recovered **mPTPM-3** powder was re-used for I₂ adsorption. The r_p was

calculated by weight gains: $r_p = c_u/394 \times 100$ wt%, where r_p is the recycling percentage and c_u is the I₂ uptake capacity of **mPTPM-3** after heating recovery. Above-mentioned iodine adsorption, release, and recycling percentage of adsorbents were average values according to three measurements.

2.3. Density functional theory (DFT) calculations

Optimizations and vibrational frequencies of eight molecular models present in **Table S5** were performed at BP86/def2-SVP level with Grimme's protocol included for empirical dispersion correction.¹⁻³ Based on the optimized structures, electron density maps were calculated by a grid size of 0.2×0.2×0.2 Å at BP86/def2-TZVP level with dispersion corrections. All calculations were carried out in TURBOMOLE 7.3 program package.⁴

3. Supplementary Figures and Tables

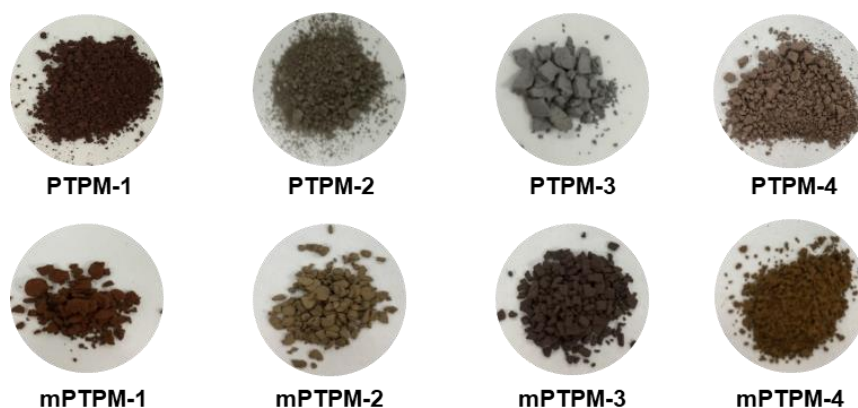


Figure S1 Appearances of PTPMs and mPTPMs.

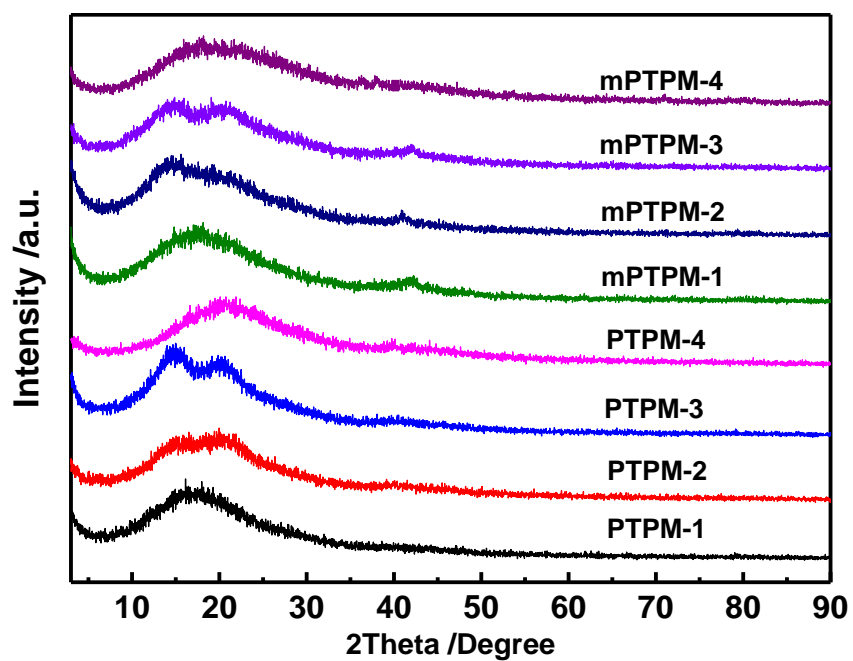


Figure S2 XRD patterns of PTPMs and mPTPMs.

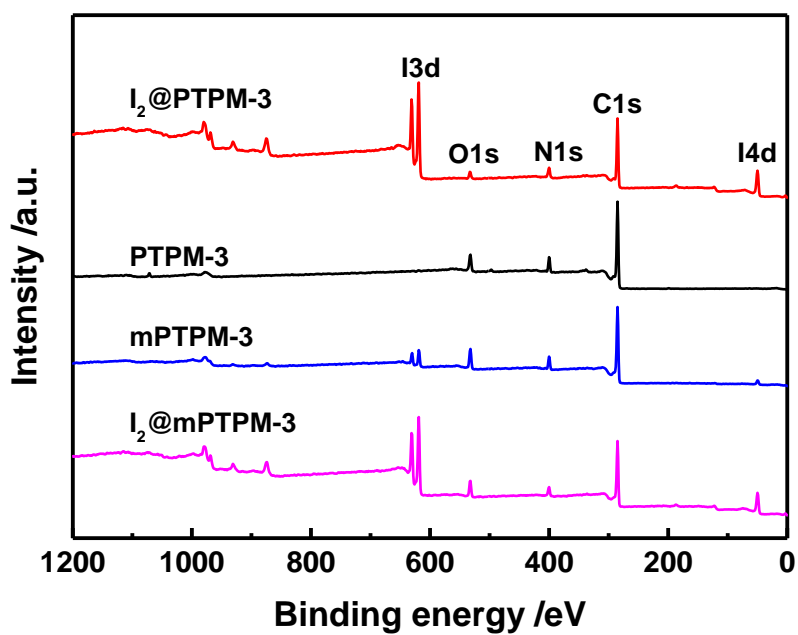


Figure S3 Full survey XPS spectra of PTPM-3, mPTPM-3, I₂@PTPM-3, and I₂@mPTPM-3.

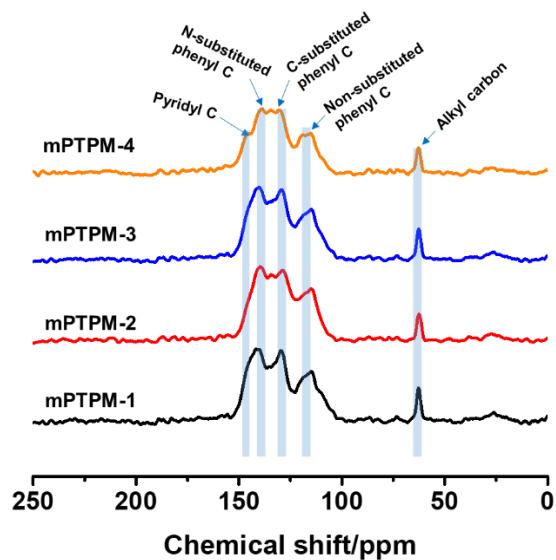


Figure S4 ^{13}C CP/MAS NMR spectra of mPTPMs.

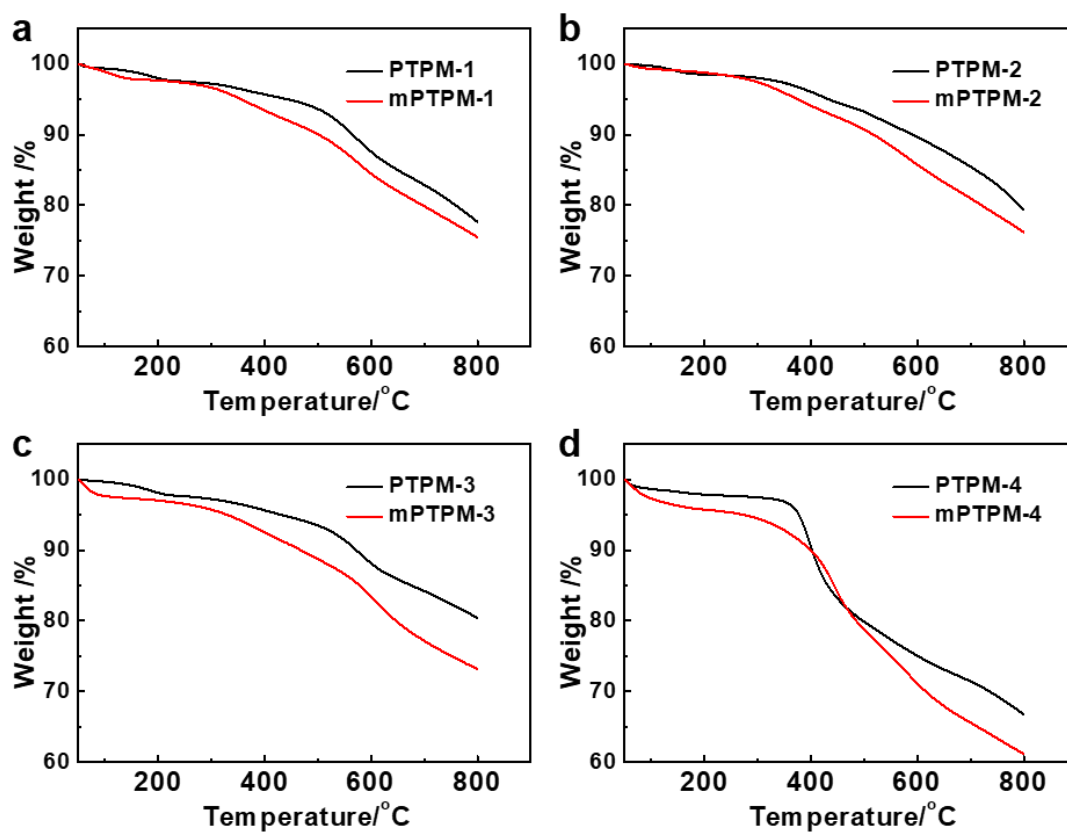


Figure S5 TGA scans of PTPMs and mPTPMs.

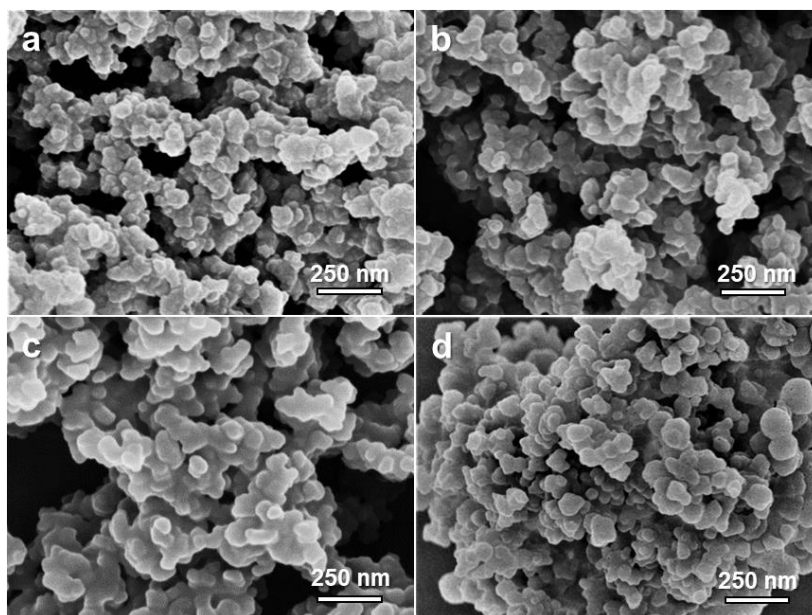


Figure S6 SEM images of (a) **PTPM-1**, (b) **PTPM-2**, (c) **PTPM-3**, and (d) **PTPM-4**.

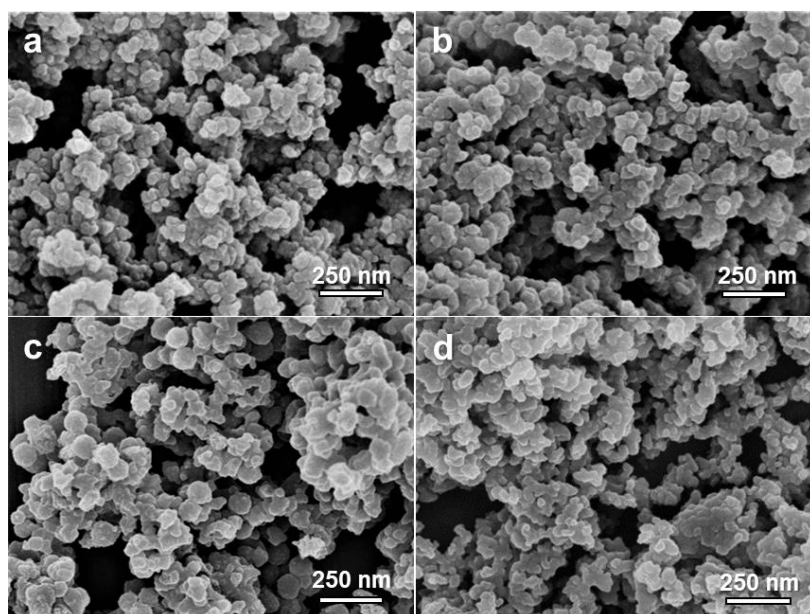


Figure S7 SEM images of (a) **mPTPM-1**, (b) **mPTPM-2**, (c) **mPTPM-3**, and (d) **mPTPM-4**.

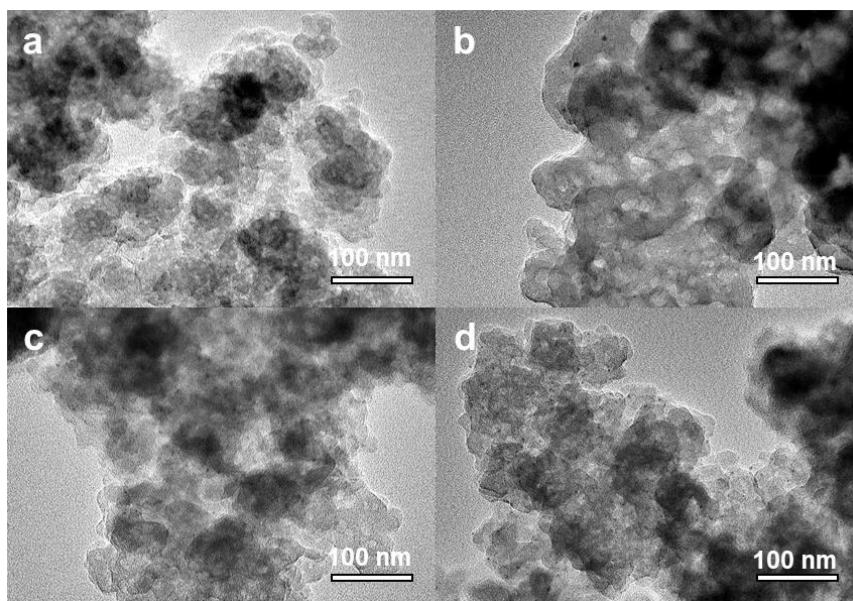


Figure S8 TEM images of (a) **PTPM-1**, (b) **PTPM-2**, (c) **PTPM-3**, and (d) **PTPM-4**.

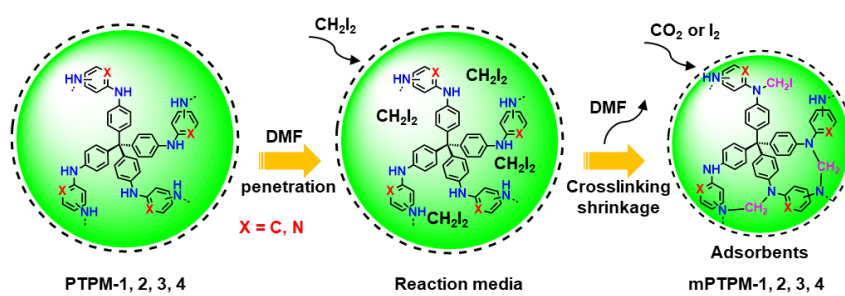


Figure S9 Schematic illustration of shrinkage effect found on the mPTPM adsorbents.

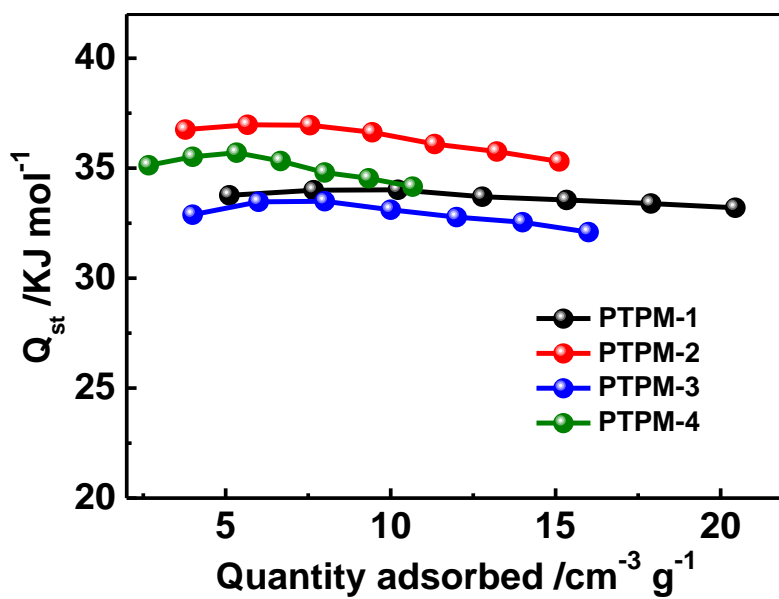


Figure S10 Heat of CO₂-adsorption of PTPMs.

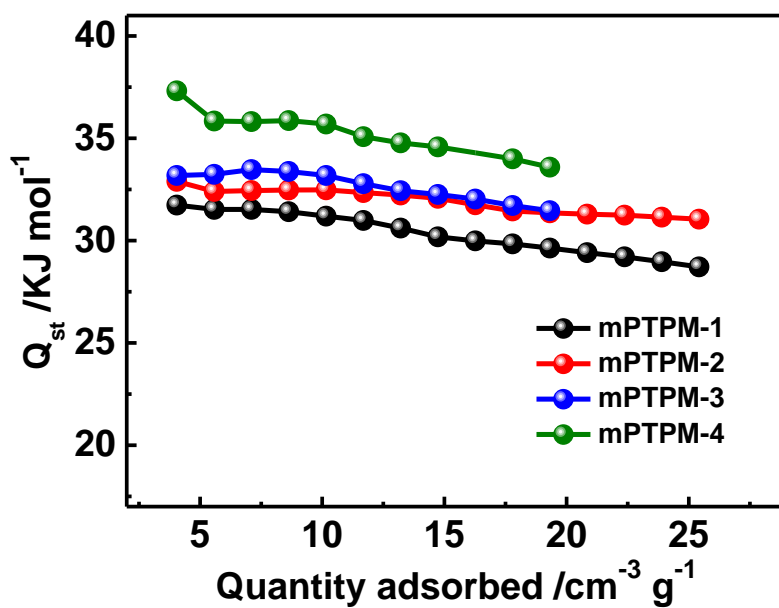


Figure S11 Heat of CO₂-adsorption of PTPMs.

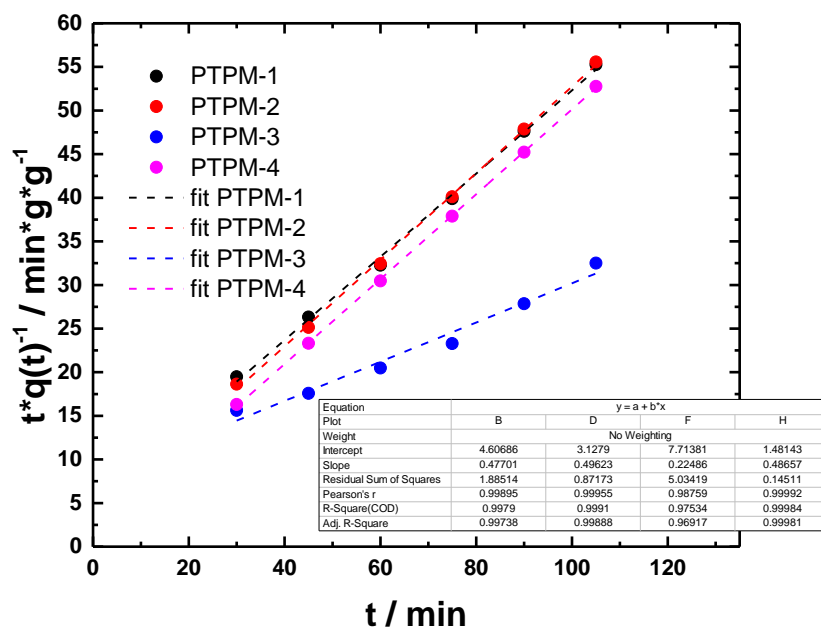


Figure S12 Pseudo-second order kinetic model of iodine uptake of PTPMs as a function of time at 358 K and ambient pressure.

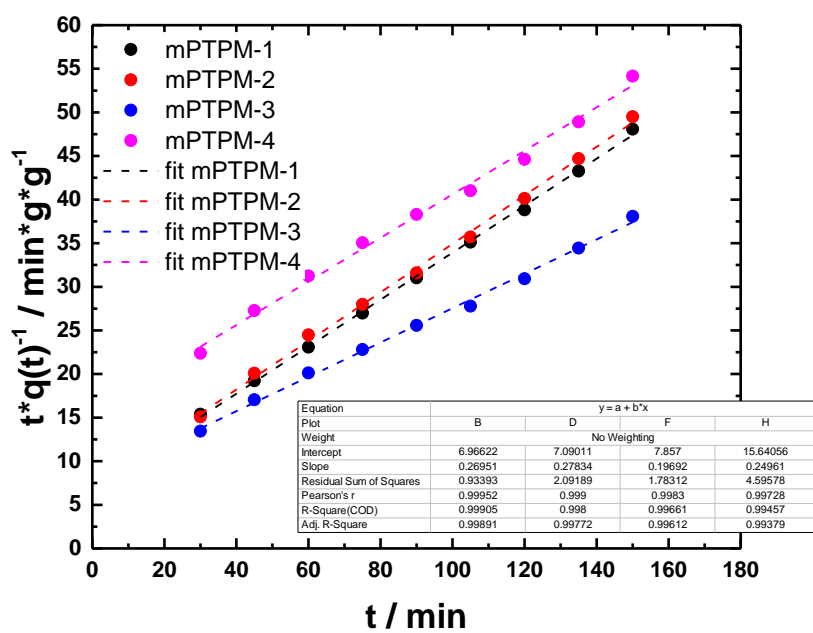


Figure S13 Pseudo-second order kinetic model of iodine uptake of mPTPMs as a function of time at 358 K and ambient pressure.

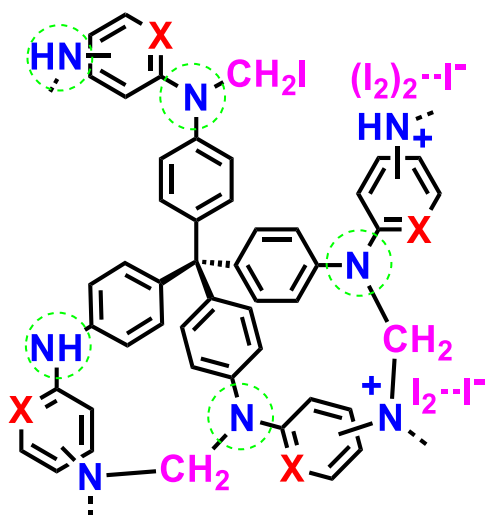


Figure S14 A chemically adsorptive model (charge transfer complex) proposed for mPTPMs and I₂ molecules.

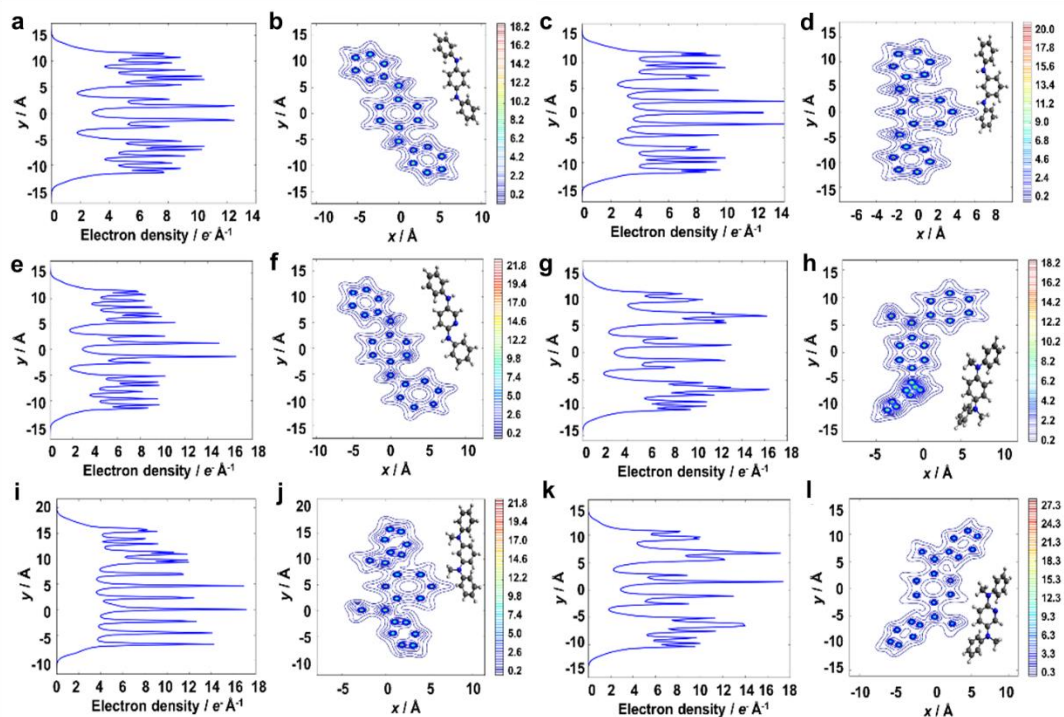


Figure S15 Electron density profiles for analogs of (a,b) **PTPM-1**, (c,d) **PTPM-2**, (e,f) **PTPM-4**, (g,h) **mPTPM-1**, (i,j) **mPTPM-2**, and (k,l) **mPTPM-4** in DFT calculations. Chemical structures are shown in the insets of (b), (d), (f), (h), (j), and (l).

Table S1 Summary of surface areas and CO₂ uptakes (273 k, 1 bar) of TPM-POPs

POPs	Surface area (m ² /g)	CO ₂ uptake (g/g ⁻¹)	Q _{st} (kJ/mol)	Reaction method	Ref.
mPTPM-2	640	0.106	32.9	Buchwald- Hartwig	This work
PIN2	325	0.079	31.0	Schiff-base	5
JUC-Z15	1570	0.078	22.6	Yamamoto	6
JUC-Z17	2144	0.088	22.1	Yamamoto	6
JUC-Z18	2334	0.090	16.5	Yamamoto	2

JUC-Z19	3137	0.109	15.7	Yamamoto	6
CPN-1-Br	1455	0.110	31.0	Yamamoto	7
IT-POP-1	245	0.075	32.9	Sonogashira- Hagihara	8
PAF-26- COOH	717	0.102	28.1	Sonogashira- Hagihara	9
LMOP-3	791	0.103	-	Heck	10
JUC-Z7	4889	0.114	15.9	Yamamoto	11
JUC-Z8	4743	0.147	18.6	Yamamoto	11
JUC-Z9	4053	0.151	19.6	Yamamoto	11
JUC-Z10	3305	0.167	23.2	Yamamoto	11
PAF-1	5341	0.090	15.6	Yamamoto	11
PA-POF-1	478	0.110	23.7	Yamamoto	12
D	1213	0.106	26.0	Sonogashira- Hagihara	3
PBO-M	745	0.116	34.4	Condensatio n	14
BCMP-1	788	0.066	-	Sonogashira- Hagihara	15
BCMP-2	490	0.067	-	Sonogashira- Hagihara	15

Table S2 Summary of structures, surface areas and I₂ uptakes of POPs

POPs	S_{BET} (m²/g)	Pressure	T (K)	Uptake time	I₂ uptake (g/g)	Ref.
mPTPM-1	513	1 bar	358	2.5 h	3.12	This work
mPTPM-2	640	1 bar	358	2.5 h	3.02	This work
mPTPM-3	278	1 bar	358	12.5 h	3.94	This work
mPTPM-4	293	1 bar	358	2.5 h	2.76	This work
NTP	1067	1 bar	348	48 h	1.80	16
PAF-23	82	1 bar	348	48 h	2.71	17
PAF-24	136	1 bar	348	48 h	2.76	17
PAF-25	262	1 bar	348	48 h	2.60	17
PAF-1	5600	40 Pa	298	10 h	1.86	18
JUC-Z2	2081	40 Pa	298	10 h	1.44	18
SCMP-II	120	1 bar	353	3 h	3.45	19
NOP-54	1178	-	348	24 h	2.02	20
CaIPOF-1	154	1 bar	348	30 h	4.06	21
CaIPOF-1	91	1 bar	348	30 h	3.53	21
1''	-	1 bar	343	10 h	0.452	22
BDP-CPP-1	635	-	348	24 h	2.83	23
BDP-CPP-2	235	-	348	24 h	2.23	23
NBDP-CPP	658	-	348	24 h	1.50	23
HCMP-3	82	1 bar	358	0.75 h	3.16	24
SCMP- 600@1	724	1 bar	350	24 h	2.04	25

SCMP- 600@2	901	1 bar	350	24 h	1.48	25
SCMP- 600@3	1042	1 bar	350	24 h	1.67	25
CTF- 1@ZnCl ₂	1476	1 bar	348	24 h	4.31	26
THPS-C	3125	1 bar	348	48 h	3.40	27
CMP-LS4	462	1 bar	353	12 h	3.32	28
CMP-LS5	1158	1 bar	353	12 h	4.40	28
CMP-LS6	679	1 bar	353	12 h	2.44	28

Table S3 Kinetic data of the iodine adsorption of PTPMs.

PTPM	slope	y-intercept	q _e [g/g]	k [g/(g*min)]	R ²
1	0.4770	4.6069	2.0964	0.0494	0.9990
2	0.4962	3.1279	2.0153	0.0787	0.9991
3	0.2249	7.7138	4.4464	0.0066	0.9753
4	0.4866	1.4814	2.0551	0.1598	0.9998

Table S4 Kinetic data of the iodine adsorption of mPTPMs.

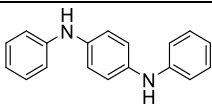
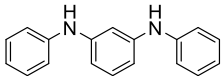
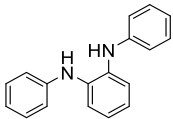
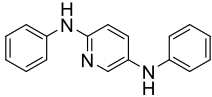
mPTPM	slope	y-intercept	q _e [g/g]	k [g/(g*min)]	R ²
1	0.2695	6.9662	3.7106	0.0104	0.9991
2	0.2783	7.0901	3.5932	0.0109	0.9980
3	0.1969	7.8570	5.0787	0.0049	0.9966
4	0.2496	15.6406	4.0064	0.0040	0.9946

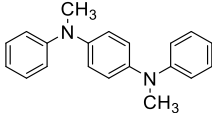
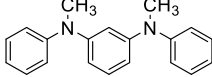
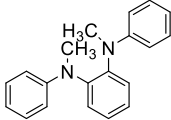
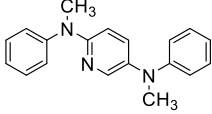
Used equation:

$$\frac{t}{q_t} = \frac{1}{k \times q_e^2} + \frac{1}{q_e} \times t$$

where q_t is the adsorbed amount at time t , q_e is the equilibrium uptake and k is the adsorption rate constant. y-Intercept is equal to $1/(k \times q_e^2)$ and the slope is equal to $1/q_e$.

Table S5 Polymers, iodine uptakes, models, and electron densities in N atoms

Polymers	I ₂ uptake (g/g)	Models	Electron densities (e ⁻ /Å)
PTPM-1	1.86		9
PTPM-2	1.85		9
PTPM-3	3.22		20
PTPM-4	1.97		11

mPTPM-1	3.12		16
mPTPM-2	3.02		17
mPTPM-3	3.94		23
mPTPM-4	2.76		12

S4. Supplementary References

1. Becke, A. D. Density-Functional Exchange-Energy Approximation with Correct Asymptotic Behavior. *Phys. Rev. A* **1988**, 38, 3098.
2. Perdew, J. P. Density-Functional Approximation for the Correlation Energy of the Inhomogeneous Electron Gas. *Phys. Rev. B* **1986**, 33, 8822.
3. Grimme, S.; Ehrlich, S.; Goerigk, L. Effect of the Damping Function in Dispersion Corrected Density Functional Theory. *J. Comput. Chem.* **2011**, 32, 1456-1465.
4. TURBOMOLE V7.2 2017, a development of University of Karlsruhe and Forschungszentrum Karlsruhe GmbH, 1989-2007, TURBOMOLE GmbH, since 2007; available from <http://www.turbomole.com>.
5. Popp, N.; Homburg, T.; Stock, N.; Senker, J. Porous Imine-Based Networks with Protonated Imine Linkages for Carbon Dioxide Separation from Mixtures with Nitrogen and Methane. *J. Mater. Chem. A* **2015**, 3, 18492-18504.

-
6. Lu, C.; Ben, T.; Qiu, S. Synthesis and Gas Storage Application of Hierarchically Porous Materials. *Macromol. Chem. Phys.* **2016**, *217*, 1995-2003.
 7. Fischer, S.; Schimanowitz, A.; Dawson, R.; Senkovska, I.; Kaskel, S.; Thomas, A. Cationic Microporous Polymer Networks by Polymerisation of Weakly Coordinating Cations with CO₂-Storage Ability. *J. Mater. Chem. A* **2014**, *2*, 11825-11829.
 8. Zhong, H.; Su, Y.; Chen, X.; Li, X.; Wang, R. Imidazolium-and Triazine-Based Porous Organic Polymers for Heterogeneous Catalytic Conversion of CO₂ into Cyclic Carbonates. *ChemSusChem* **2017**, *10*, 4855-4863.
 9. Ma, H.; Ren, H.; Zou, X.; Meng, S.; Sun, F.; Zhu, G. Post-Metalation of Porous Aromatic Frameworks for Highly Efficient Carbon Capture from CO₂ + N₂ and CH₄ + N₂ Mixtures. *Polym. Chem.* **2014**, *5*, 144-152.
 10. Sun, L.; Liang, Z.; Yu, J.; Xu, R. Luminescent Microporous Organic Polymers Containing the 1, 3, 5-Tri(4-ethenylphenyl)benzene Unit Constructed by Heck Coupling Reaction. *Polym. Chem.* **2013**, *4*, 1932-1938.
 11. Pei, C.; Ben, T.; Li, Y.; Qiu, S. Synthesis of Copolymerized Porous Organic Frameworks with High Gas Storage Capabilities at Both High and Low Pressures. *Chem. Commun.* **2014**, *50*, 6134-6136.
 12. Liu, Y.; Landskron, K. Anionic Porous Organic Frameworks as Advanced Functional Adsorbents for CO₂ and Organic Micropollutants in Water. *J. Mater. Chem. A* **2017**, *5*, 23523-23529.
 13. Dawson, R.; Stöckel, E.; Holst, J. R.; Adams, D. J.; Cooper, A. I. Microporous Organic Polymers for Carbon Dioxide Capture. *Energy Environ. Sci.* **2011**, *4*, 4239-4245.
 14. Zhang, B.; Yan, J.; Wang, Z. Microporous Polybenzoxazoles with Tunable Porosity

-
- and Heteroatom Concentration for Dynamic Adsorption/Separation of CO₂ Mixed Gases. *J. Phys. Chem. C* **2018**, *122*, 12831-12838.
15. Shi, Q.; Sun, H.; Yang, R.; Zhu, Z.; Liang, W.; Tan, D.; Deng, W. Synthesis of Conjugated Microporous Polymers for Gas Storage and Selective Adsorption. *J. Mater. Sci.* **2015**, *50*, 6388-6394.
16. Ma, H.; Chen, J. J.; Tan, L.; Bu, J. H.; Zhu, Y.; Tan, B.; Zhang, C. Nitrogen-Rich Triptycene-Based Porous Polymer for Gas Storage and Iodine Enrichment. *ACS Macro Lett.* **2016**, *5*, 1039-1043.
17. Yan, Z.; Yuan, Y.; Tian, Y.; Zhang, D.; Zhu, G. Highly Efficient Enrichment of Volatile Iodine by Charged Porous Aromatic Frameworks with Three Sorption Sites. *Angew. Chem. Int. Ed.* **2015**, *54*, 12733-12737.
18. Pei, C.; Ben, T.; Xu, S.; Qiu, S. Ultrahigh Iodine Adsorption in Porous Organic Frameworks. *J. Mater. Chem. A* **2014**, *2*, 7179-7187.
19. Ren, F.; Zhu, Z.; Qian, X.; Liang, W.; Mu, P.; Sun, H.; Li, A. Novel Thiophene-bearing Conjugated Microporous Polymer Honeycomb-like Porous Spheres with Ultrahigh Iodine Uptake. *Chem. Commun.* **2016**, *52*, 9797-9800.
20. Chen, D.; Fu, Y.; Yu, W.; Yu, G.; Pan, C. Versatile Adamantane-based Porous Polymers with Enhanced Microporosity for Efficient CO₂ Capture and Iodine removal. *Chem. Eng. J.* **2018**, *334*, 900-906.
21. Su, K.; Wang, W.; Li, B.; Yuan, D. Azo-Bridged Calix[4]resorcinarene-Based Porous Organic Frameworks with Highly Efficient Enrichment of Volatile Iodine. *ACS Sustainable Chem. Eng.* **2018**, *6*, 17402-17409.
22. Deshmukh, M. S.; Chaudhary, A.; Zolotarev, P. N.; Boomishankar, R. A 3D Coordination Network Built from Cu^{II}₄Cl₃(H₂O)₂ Linear Clusters and Tetrapyridyl Tetrahedral Silane Ligands: Reversible Iodine Uptake and Friedel–Crafts

-
- Alkylation Reactions. *Inorg. Chem.* **2017**, *56*, 11762-11767.
23. Zhu, Y.; Ji, Y. J.; Wang, D. G.; Zhang, Y.; Tang, H.; Jia, X. R.; Kuang, G. C. BODIPY-Based Conjugated Porous Polymers for Highly Efficient Volatile Iodine Capture. *J. Mater. Chem. A* **2017**, *5*, 6622-6629.
24. Liao, Y.; Weber, J.; Mills, B. M.; Ren, Z.; Faul, C. F. Highly Efficient and Reversible Iodine Capture in Hexaphenylbenzene-Based Conjugated Microporous Polymers. *Macromolecules* **2016**, *49*, 6322-6333.
25. Liu, M.; Yao, C.; Liu, C.; Xu, Y. Thiophene-Based Porous Organic Networks for Volatile Iodine Capture and Effectively Detection of Mercury Ion. *Sci. Rep.* **2018**, *8*, 14071.
26. He, X.; Zhang, S. Y.; Tang, X.; Xiong, S.; Ai, C.; Chen, D.; Yu, G. Exploration of 1D Channels in Stable and High-Surface-Area Covalent Triazine Polymers for Effective Iodine Removal. *Chem. Eng. J.* **2019**, *371*, 314-318.
27. Zhang, Q. M.; Zhai, T. L.; Wang, Z.; Cheng, G.; Ma, H.; Zhang, Q. P.; Zhang, C. Hyperporous Carbon from Triptycene-Based Hypercrosslinked Polymer for Iodine Capture. *Adv. Mater. Interfaces* **2019**, 1900249.
28. Wang, S.; Liu, Y.; Ye, Y.; Meng, X.; Du, J.; Song, X.; Liang, Z. Ultrahigh Volatile Iodine Capture by Conjugated Microporous Polymer Based on N, N, N', N'-tetraphenyl-1, 4-phenylenediamine. *Polym. Chem.* **2019**, *10*, 2608-2615.